arXiv:1404.3072v1 [astro-ph.GA] 11 Apr 2014

The Catalog of Edge-on Disk Galaxies from SDSS. Part I: The Catalog and the Structural Parameters of Stellar Disks

Bizyaev, D. V.[1,2] , Kautsch, S. J.[3], Mosenkov, A. V.[4,5], Reshetnikov, V.P. [5,6], Sotnikova, N. Ya.[5,6], Yablokova, N. V.[5], and Hillyer, R.W.[7]

ABSTRACT

We present a catalog of true edge-on disk galaxies automatically selected from the Seventh Data Release (DR7) of the Sloan Digital Sky Survey. A visual inspection of the g, r and i images of about 15000 galaxies allowed us to split the initial sample of edge-on galaxy candidates into 4768 (31.8% of the initial sample) genuine edge-on galaxies, 8350 (55.7%) non-edge-ons, and 1865 (12.5%) edge-on galaxies not suitable for simple automatic analysis because these objects show signs of interaction, warps, or nearby bright stars project on it. We added more candidate galaxies from RFGC, EFIGI, RC3, and Galaxy Zoo catalogs found in the SDSS footprints. Our final sample consists of 5747 genuine edge-on galaxies. We estimate the structural parameters of the stellar disks (the stellar disk thickness, radial scale length, and central surface brightness) in the galaxies by analyzing photometric profiles in each of the g, r, and i images. We also perform simplified 3-D modeling of the light distribution in the stellar disks of edge-on galaxies from our sample. Our large sample is intended to be used for studying scaling relations in the stellar disks and bulges and for estimating parameters of the thick disks in different types of galaxies via the image stacking. In this paper we present the sample selection procedure and general description of the sample.

Subject headings: galaxies: structure, galaxies: edge-on

1. Introduction

Edge-on galaxies provide a unique opportunity for studying the vertical structure of galactic components. Starting from early studies conducted mostly in the optical bands (Kormendy & Bruzual 1978; Burstein 1979; van der Kruit & Searle 1981a,b; Kylafis & Bahcall 1987) using simple photometric profile fitting, the studies of the vertical structure of galactic components evolved towards complex modeling based on the radiation transfer methods (Xilouris et al. 1999; Yoachim et al. 2006; Bianchi 2007; Baes et al. 2011; Schechtman-Rook et al. 2012; De Geyter et al. 2013) using multiple UV, optical and IR data (Popescu et al. 2000; De Geyter et al. 2013). Most of the structural studies employed limited samples of objects using high quality observations. Large surveys conducted during the last decade have made available benefits of observing large samples of interesting objects, which helps in statistical studies of the vertical structure of galactic disks, bulges, and thick disks (Zibetti et al. 2004; Bergvall et al. 2010). In this paper we describe our approach to selection of true edge-on galaxies from objects observed by Sloan Digital Sky Survey (Aihara et al. 2011, SDSS). We identified about six thousand genuine edge-on galaxies with inclination angles not more than a few degrees different from perfect edge-on view. Our sample allows statistical studies of the vertical

[1]Apache Point Observatory and New Mexico State University, Sunspot, NM, 88349, USA

[2]Sternberg Astronomical Institute, Moscow State University, Moscow, Russia

[3]Nova Southeastern University, Fort Lauderdale, FL, 33314, USA

[4]Central Astronomical Observatory of RAS, Russia

[5]St. Petersburg State University, Russia

[6]Isaac Newton Institute of Chile, St. Petersburg Branch

[7]Christopher Newport University, Newport News, VA, 23606, USA

structure parameters of galactic components for the largest sample known to date. We also introduce an on-line catalog of processed SDSS images and of corresponding structural parameters, which will simplify further studies of edge-on disk galaxies in the optical bands. This paper describes our sample selection procedure and our approach to determination of the stellar disk parameters. The paper is focused mostly on the stellar disk parameters, while bulges will be considered in the next paper.

2. The Sample of Edge-on Galaxies

2.1. Selection of Candidates to the Initial Sample

The initial sample of candidates to edge-on galaxies was automatically selected from the SDSS DR7 (Abazajian et al. 2009) using its Catalog Access Server query tools. The selection criteria are discussed in detail by Kautsch et al. (2006a,b); Kautsch (2009). This selection was based on the axial ratio, angular diameter, magnitude and color limits. Flagged galaxies and objects with extreme magnitude errors we not included. The SDSS query was taylored to select relatively bright galaxies with apparent Petrosian magnitudes in the g band less than 20 mag using the Petrosian flux; galaxies with angular major-axis diameters larger than 30 arcsec based upon isoA_g, the isophotal major axis given in SDSS in g band; and "flat" galaxies with axis ratio greater than 3 in the g-band, which is defined by the isophotal axes isoA_g divided by isoB_g. The objects are also selected in certain (-0.5 $\leq$ g-r $\leq$ 2) and (-0.5 $\leq$ r-i $\leq$ 2) color ranges. The use of the color ranges in reddening-corrected Petrosian magnitudes allows to prevent the inclusion of galaxies with unusual colors caused by AGNs, instrument flaws, or ghost images. All these selection criteria were applied to the Galaxy table (G.) at the SDSS SkyServer using Structured Query Language (sql). The sql query follows:

```
petroMag_g < 20
G.isoA_g/G.isoB_g > 3
-0.5 <  G.dered_g - G.dered_r < 2
-0.5 <  G.dered_r - G.dered_i < 2
G.isoA_g > 37.8
```

The resulting sample consisted of 18277 unique objects. A brief visual inspection of the images was done to get rid of false detections. After that, our final sample of the *candidates* to edge-on galaxies included 14983 objects.

2.2. Visual Inspection and the Final Sample of True Edge-on Galaxies

The photometrically calibrated SDSS frames with selected candidates in the g, r, and i bands were taken from the SDSS Data Access Server. By the time we started working with the images, SDSS Data Release 8 was issued (Aihara et al. 2011), and the images were downloaded from the DR8. The images were cleaned of foreground stars. The star candidates were identified in the images as objects with FWHM from 1 to 1.5 arcsec (typical values during the SDSS imaging campaign, Abazajian et al. (2009)). The stars in the images were replaced by the median values of pixels beyond 3 arcsec (about twice the typical FWHM) from their center. Since the selected images from SDSS are far from really crowded fields, this method of cleaning from stars did not produce strong artifacts. Just a few cases of projected bright stars were caught in the course of the visual inspection and such galaxies were removed from the consideration. The very central regions of the galaxies were excluded from the cleaning procedure. Having initial guess about the galactic center coordinates, we fitted ellipses to galactic isophotes at the level of signal-to-noise S/N = 2 per pixel (with the image scale of approximately 0.4 arcsec per pixel). Fitting ellipse to the outer galactic isophotes allowed us to adjust the position of the galactic center and to determine the size of the "region of interest" that encompasses the whole galaxy (the encompassing ellipse, hereafter). The images then were rotated to align the major axis of the encompassing ellipse with the X-axis in the new subframes, and then cropped. This allowed us to make a set of images with known geometrical parameter centered on the galaxies, which is necessary for the further automatic processing (see §3). The images were used for simplification of our visual inspection and also became a part of our catalog (see §3.3).

As the next step, all objects were visually classified into groups from the standpoint of further availability for automatic processing. The galax-

ies with clearly seen dust layer, or without signs of non-edge-on spiral arms were classified as true edge-ons. As a result, we selected groups of genuine edge-on galaxies, non edge-ons, objects that needed manual pre-processing (e.g. because a bright star nearby did not allow automatic algorithm to determine parameters of the galaxy correctly), and objects that are not suitable for the automatic processing described below. In other words, we excluded the objects whose galactic midplane cannot be aligned along the major axis of a subimage. The latter group includes significantly warped edge-on galaxies, and interacting galaxies. This group also includes galaxies with with very bright projected stars, whose subtraction would modify significant part of the galactic image. The initial frames with the objects for the manual processing were then inspected visually, the centers of the galaxies and their orientation parameters were estimated and properly rotated subframes were made. The galaxies then were classified in the way described above and added to the main sample. The resultant sample was split into 4768 (31.8%) true edge-on galaxies, 8350 (55.7%) non-edge-ons, and 1865 (12.5%) of those objects that need a more complex analysis. We do not consider the latter group of the objects in this paper. The non-edge-on galaxies were also excluded from the further consideration. This paper is focused on the analysis of the structural parameters of bona fide edge-on, non warped and non interacting, galaxies.

The galaxies were classified into obvious morphological types, from Sa to Irr using an automatic algorithm, which was described in detail by Kautsch et al. (2006a); Kautsch (2009). The major goal of this classification is to assign morphological Hubble types based upon the size of the bulge component since other morphological properties such as the shape of spiral arms are obscured at the edge-on view. We use the concentration index and the ellipticity of the objects for making this automated classification.

The concentration index (CI) is widely used as a classification criterion, reflecting a measure of the spheroidal component in galaxies (e.g., Pranger at al. (2012); Strateva et al. (2001)). We used the CI provided by the SDSS. It is defined as the ratio of the Petrosian radii (petrorad) that contain 90 and 50 % of the petrosian flux in the r band (Stoughton et al. 2002). The CI in SDSS is measured using circular apertures. This leads to a significant flaw in classification of galaxies with a wide range of viewing angles in surveys that observe all types of galaxies with different inclinations ranging from face-on to edge-on view. In our work we focus on purely edge-on disk galaxies. This, in turn, means that all our objects are affected in the same way, and we do not have to deal with normalizing inclination effects to the CI since our sample is carefully selected to consist of only edge-on galaxies. Kautsch et al. (2006a) found that the CI clearly separates galaxies with an apparent bulge from galaxies without a clear bulge component.

The CI separation values are chosen by visual classification and then have been applied to serve as the limiting values for automated classification. However, pure simple disk galaxies were not detected in a satisfying way so that Kautsch et al. (2006a) introduced a second measure which allowed to select bulgeless disks without any central spheroidal component. This parameter reflects the ellipticity (e) of the galaxies, and was based on luminosity weighed elliptical isophotes. Also in this case Kautsch et al. (2006a) used visual classification to find the best limiting values in order to distinguish the morphological classes according to the eye inspection. The separation of the morphological types is necessarily somewhat arbitrary, and this is in the nature of the classification itself. Kautsch et al. (2006a) choose the limits based on visual classification and applied those to the automatic cataloging, and they also were required to be consistent with similar studies (Karachentsev et al. 1993, 1999). Therefore, our classification should act as an indicator of the dominance of the bulge component translated into the common language of Hubble types. Later (in Fig. 8) we will see that the classification reflects the Bulge/Total ratios derived from the 1-D profile fitting, which confirms the classification method described above.

In Table 1 and Table 2 we provide the limiting values of CI and ellipticity, as well as their mean values. Note that the catalog contains a significant number of early-type spirals because we did not limit our selection to flat and bulgeless, late-type spirals due to our choice of selection criteria as discussed in section 2.1. A summary of the frac-

tion of different morphological types in the sample is shown in Table 3.

Since the initial automatic selection of the galaxy candidates did not include significant number of the largest edge-on galaxies, we incorporated more edge-on candidates by supplying objects from the Revised Flat Galaxy Catalog (Karachentsev et al. 1999, RFGC, hereafter), RC3 de Vaucouleurs et al. (1991), EFIGI (Baillard et al. 2011), and GalaxyZoo (Lintott et al. 2011) that were found in the SDSS footprints. The reason for missing extended objects in the SDSS fields lies in the difficulty to assign correct borders to large and extended objects with multiple luminosity centers, e.g., HII regions. This so-called shredding causes that those missed galaxies are detected as two or more entries by SDSS's image processing pipeline.

Only the galaxies with major axis greater than 30 arcsec (according to the HyperLeda database, Paturel et al. (2003)) were added. All new edge-on candidates were processed in the way described above and then visually inspected. The final sample of unique true edge-on galaxies consists of 5747 objects. Fig. 1 shows that the galaxies in our sample are more or less uniformly allocated in the SDSS imaging survey area.

We checked the completeness of our catalog using the recipes by Thuan & Seitzer (1979). Their V/V_m value was calculated for the whole sample and we found that our genuine edge-on subsample is 95 % complete for all galaxies with major axis size larger than 28 arcsec. Fig. 2 shows the histogram of the distribution of the major axes, top curve. Our morphological classification allows for splitting the histogram by types, which is shown in

Table 1: Concentration index classification criteria and observing values.

Type	Lower Limit	Upper Limit	Mean, error
Sa	2.70	–	3.191 ± 0.011
Sab, Sb	2.70	–	2.990 ± 0.005
Sc	2.15	2.70	2.540 ± 0.005
Scd	2.15	2.70	2.498 ± 0.007
Sd	–	2.70	2.403 ± 0.005
Irr	–	2.15	1.894 ± 0.030

Table 2: Ellipticity classification criteria and observing values.

Type	Lower Limit	Upper Limit	Mean, error
Sa	–	0.400	0.310 ± 0.004
Sab, Sb	0.400	–	0.666 ± 0.003
Sc	–	0.766	0.713 ± 0.003
Scd	0.766	0.816	0.794 ± 0.002
Sd	0.816	–	0.826 ± 0.003
Irr	–	0.816	0.367 ± 0.004

Table 3: Edge-on galaxies in our sample by morphological types.

Type	Fraction, Percent
Sa	7.2%
Sab, Sb	32.2%
Sc	19.2%
Scd	10.8%
Sd	28.8%
Irr	1.8%

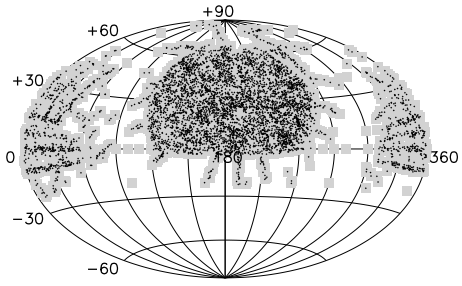

Fig. 1.— The distribution of genuine edge-on galaxies in the sky shows that they cover RA-Dec space essentially the same way as all SDSS objects do, according to Aihara et al. (2011) and sdss3.org. The grey shaded area designates the SDSS imaging footprints.

Fig. 2. Galaxies of different morphological types observed edge-on may be affected by dust on a different way, but we see that different types follow the general distribution. We also calculated the Thuan & Seitzer's V/V_m in dependence of the morphological types and found that the Sa, Sb, Sc, Scd, and Sd types are 95% complete for the galaxies with the major axes greater than 33, 28, 26, 25, and 27 arcsec, respectively. The Irr subsample has low statistics not enough for certain V/V_m calculation. Thus, we conclude that the completeness is not a strong function of the morphological type.

We performed a test how well we select the true edge-on galaxies among objects with arbitrary inclination. For this purpose we submitted a DR7 CAS query with the same sample selection criteria except the axis ratio limit. As a result, the output comprises 161571 objects. The inclination angle i was coarsely estimated from the minor-to-major axes ratio (b/a) using equation $\cos^2(i) = ((b/a)^2 - q^2)/(1 - q^2)$ (Hubble 1926), where we assume that the intrinsic axial ratio in the galactic disks is the same for all objects and is equal to $q = 0.13$ (Giovanelli et al. 1994), and the major and minor axes a and b are the r-band sizes from the DR7 CAS tables. Fig. 3 shows the distribution of the *formally* estimated $\cos(i)$, which has to be flat in the case of equal probability of the galactic inclinations in space. Fig. 3 demonstrates that the variety of edge-on galaxies cannot be described by a single universal value of the internal flatness q. It is seen that due to contamination from non-edge-on galaxies with the inclination between 80 and 86 degrees the inclination distribution strongly peaks at 90 degrees. At the same time, the object migration to the peak creates the dip between 80 and 86 degrees.

Our visual inspection allowed us to select statistically reasonable sample of true edge-on galaxies: assuming that we classify a galaxy as a genuine edge-on if its inclination is over 86 degrees (de Grijs et al. 1997; Bizyaev & Kajsin 2004), the corresponding number is calculated from the size of our true-edge-on sample and is designated by the lower short bar at 86-90 degrees in Fig. 3. The upper short bar shows the number of the galaxies in our full resulting sample (i.e. the sample with further additions beyond the automatic CAS SDSS selection). The shape of the distribution is the same as in other studies based on SDSS samples, e.g. as in Masters et al. (2010). Note that the peak at the left side of the distribution (where cos(i) is close to 1) shows growing contribution of elliptical galaxies to the general sample. This does not affect the high-inclination end of the diagram. Note that Fig. 3 is the illustration only that shows selection effects in the case if an oversimplified approach to the inclination determination is applied. The procedure of our visual inspection provides a more robust way of selection of the edge-on galaxies.

3. The Structural Parameters from the 1-D analysis of Photometric Profiles

We performed the analysis of 1-D photometric profiles using the same technique as described by Bizyaev & Mitronova (2002, 2009). The volume brightness in the stellar disks is assumed to change as follows in the radial r and vertical z directions:

$$\rho_L(r, z) = \rho_{L_0} \exp(-r/h) \operatorname{sech}^2(z/z_0), \quad (1)$$

where h is the scalelength and z_0 is the scaleheight of the disk. The central face-on disk luminosity $I_0 = \int_{-\infty}^{\infty} \rho(0, z)dz$ corresponds to the central surface brightness S_0. The model photometric profiles are obtained by the integration of equation (1) along the line-of-sight and by the convolution with the instrumental profile. We assume that the point spread function (PSF) is equal to 1.4 arcsec for all considered images, given the survey photometry campaign description (Aihara et al. 2011). The central regions of the galaxies (1/4 of the semi-major axis of the encompassing ellipse) in which bulges can be seen are excluded from the stellar disk parameters evaluation in all galaxies. The best-fit scales and surface brightness are estimated from the radial or vertical profiles that were drawn through each pixel row and column within the encompassing ellipses in the cleaned and rotated subframes. Although we did not take the the inclination angle into account in this 1-D approach, our visual inspection should select the galaxies with small deviation from the 90-degrees inclination. As it has been shown by Barteldrees & Dettmar (1994); de Grijs (1998); Kregel et al. (2002), the small deviation from the perfect edge-on view does not affect the structural parameters significantly.

We also evaluate and find the structural parameters separately in two halves of the galactic

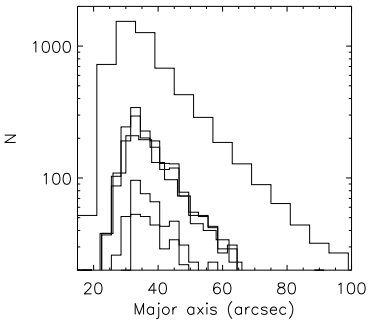

Fig. 2.— The distribution of the galactic major axis size that was estimated from the SDSS images at S/N=2 level, see text. The distribution (top curve) suggests that our sample is complete for the galaxies with the major axis greater than 28 arcsec. Different morphological types are shown below the general sample and correspond to Sb, Sd, Sc, Scd, and Sa from top to bottom, respectively.

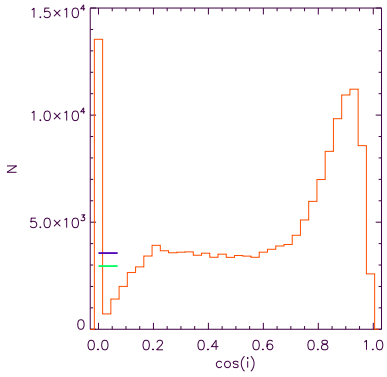

Fig. 3.— Cosine of the inclination angle in the galaxies selected from SDSS DR7 formally estimated from the major-to-minor axes ratio (see text) is shown as the solid line histogram. The lower short bar at the highest inclinations designates the number of our true edge-on galaxies estimated from the objects selected with SDSS CAS query. The upper short bar designates the total number of the real edge-on galaxies in our final sample.

images (as seen above and below the galactic midplane) . An axisymmetric and dustless galaxy, even observed at a small angle with respect to the perfect edge-on view, will have the same brightness for the parts seen above and below the galactic midplane. In the presence of dust extinction the galaxy's halves above and below the midplane look different for observers, see e.g. Xilouris et al. (1999); Bianchi (2007). To mitigate effects of the dust, we consider the scales and surface brightness only for the brightest half of each galaxy. Note that because of our selection procedure there is no big difference between the parameters determined from the brightest half only and from the entire galaxy. The output structural parameters reported by us are the median values of all considered photometric profiles.

Once the structural parameter difference in the NIR photometric bands is affected by the dust attenuation (Bizyaev & Mitronova 2009), the difference in the optical bands is affected also by the gradients of the stellar population. This makes us consider the structural parameters in the g, r, and i bands separately from each other.

We also coarsely estimate the contribution of the bulge to the luminosity of the galaxies. Using the estimated S_0, h, and z_0, we create images of edge-on disks, and subtract them from the images of the galaxies. The bulge-to-total luminosity ratio is found as the luminosity of the residual image integrated over the region within 1.0 h from the center normalized by the total luminosity of the galaxy integrated within the encompassing ellipse. The structural parameters estimated from the 1-D profile analysis for our sample of genuine edge-on galaxies are shown in Table 4.

Comparison with the RFGC shows that our catalog has 917 RFGC objects. The vertical and radial sizes of the encompassing ellipses well correlate with the size of the galaxies visually estimated in RFGC: our r-band semimajor axis size is 0.95 $\pm$ 0.13 of the red semimajor axis for the common galaxies, and our semi minor size is 1.27 $\pm$ 0.21 of the semiminor axis for them. We matched our catalog to the sample by Bizyaev & Mitronova (2009) and found 53 objects in common. Our h and z_0 well correlate with the same structural parameters determined by Bizyaev & Mitronova (2009) for those 53 galaxies: on average, our radial scale length in the i is 1.11 $\pm$ 0.43 of that in the J band,

and the vertical scale height is 1.20 ± 0.15 of the J-band scale from Bizyaev & Mitronova (2009). A little worse agreement is for 20 common galaxies with Mosenkov et al. (2010): the ratio of our scale length to the published one is 1.11 ± 0.25, and the ratio of the scale heights is 1.42 ± 0.41 for the J-band images.

Sample by Yoachim et al. (2006) has 18 common galaxies with our catalog. Our structural parameters were determined using the same functional form for the radial and vertical profiles, and the results are in reasonable agreement: our radial scale length is 1.23 ± 0.30, and our vertical scale height is 0.99 ± 0.13 of those from the R-band estimates by Yoachim et al. (2006).

The parameters for one common with Pohlen et al. (2004) thick early type disk galaxy are also in a good agreement (1.03 and 1.07 for the radial and vertical scales ratio, respectively, between our g and their V images). Our scale length is 1.07 ± 0.36 of that found for the large galaxies by Bianchi (2007). On the other hand, our scale height is much thicker than that reported by Bianchi (2007).

3.1. The Structural Parameters

The histogram of the distribution of the radial-to-vertical scale ratios h/z_0 is shown in Fig. 4. The distribution has a prominent peak at $h/z_0 \approx 2.5$ in the r band. The median values over the whole sample are 3.6, 3.4, and 3.3 for the g, r, and i bands, respectively. The radial-to-vertical scale ratios in Fig. 4 are somewhat lower than those for the typical edge-on galaxies estimated from the NIR (Bizyaev & Mitronova 2002, 2009). For the sample of 153 galaxies composed by Bizyaev & Mitronova (2002) the median ratio of h/z_0 is about 4.8. This is expected because we do not constrain the bulge contribution and consider a wide range of disk galaxies (see Fig. 6), whereas Bizyaev & Mitronova (2002, 2009) focused on bulgeless galaxies. The scale ratios in our sample are consistent with the NIR data presented by Mosenkov et al. (2010). Mosenkov et al. (2010) constructed a sample of 175 edge-on galaxies both of early- and late-types and found the median ratio h/z_0 to be about 3.5 in the J band and 3.9 for the H and K_s bands.

The distribution of the face-on central surface brightness S_0 in the gri bands is shown in Fig. 5. The surface brightness was corrected for reddening in our Galaxy using the extinction maps by Schlegel et al. (1998). It is seen that the central surface brightness values S_0 span five magnitudes in each band. Apparently, our central surface brightness is biased towards the dimmer values with respect to those for arbitrary inclined galaxies, which is a manifestation of the dust extinction within the galaxies. It suggests that a more complex modeling will help in better recovery of the stellar disk central brightness from the data of optical photometry.

Although the bulge contribution is a parameter affected by dust and projection effects in edge-on galaxies, the bulge-to-disk luminosity ratio is helpful in morphological classification since the spiral arms cannot be observed in edge-on stellar disks. We show the B/T ratio for the galaxies in our sample in Fig. 6 with a warning of using this value with caution for direct comparison with arbitrary inclined galaxies. A more honest B/T ratio can be recovered from 3-D modeling with including the central area of galactic images into analysis. The inverse scale ratio h/z_0 reveals some dependence of the bulge-to-total ratio, whereas our 3-D analysis shows that the trend is much less significant.

The disk central surface brightness determined for the brighter and dimmer halfs of the galaxies allows us to introduce the "brightness asymmetry" parameter estimated as the difference between the brighter and the dimmer values of the central surface brightness. Although it is a function of the galactic inclination in the case of an individual galaxy, in a combination with variable disk thickness, bulge strength, and clumpy nature of the dust layer it is not a direct measure of the inclination in a sample of edge-on galaxies. Nevertheless, the asymmetry gives a possibility to test if our selection procedure is biased and gives preference to certain values of the asymmetry. We ran the V/V_m test as in §2.2 for several groups of galaxies with similar asymmetry Asy in the r-band: $0 < Asy < 0.14\,mag$, $0.14\,mag < Asy < 0.30\,mag$, $0.30\,mag < Asy < 0.49\,mag$, $0.49\,mag < Asy < 0.75\,mag$, and $Asy > 0.75\,mag$. Each of the five groups contains approximately equal number of the members, which is 1/5 of the whole sample. The 95% completeness level is achieved for the major axis greater than 30, 29, 29, 28, and 27 arcsec,

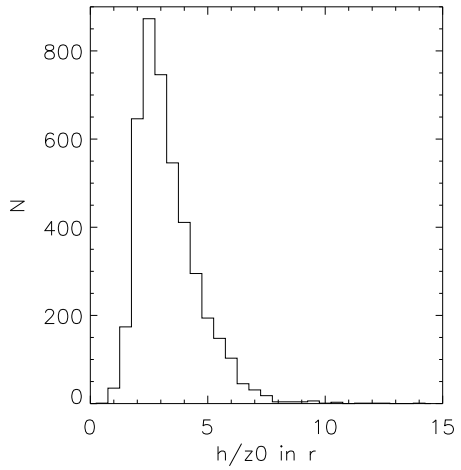

Fig. 4.— The distribution of the inverse stellar disk thickness h/z_0 estimated from the r-band images for all galaxies whose z_0 is greater than 3 pixels.

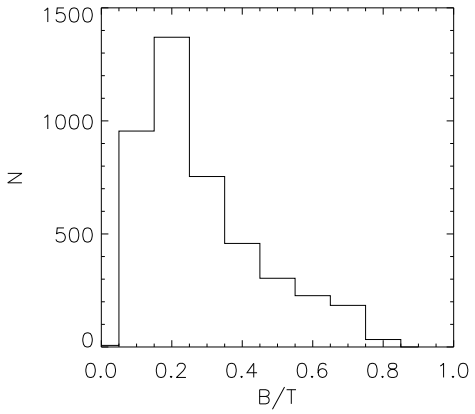

Fig. 6.— The distribution of the bulge-to-total luminosity ratio B/T. The ratio is estimated from the r-band images of all galaxies whose z_0 is greater than 3 pixels.

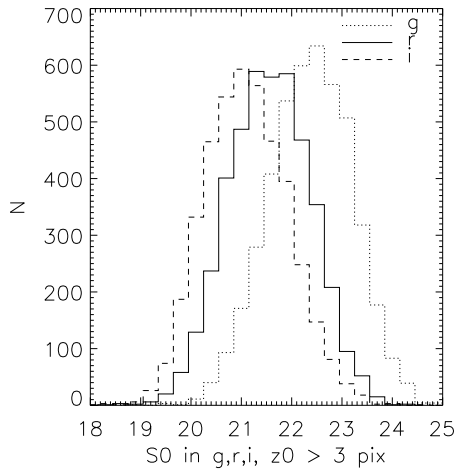

Fig. 5.— The distribution of the stellar disk's central face-on surface brightness. The dotted, solid, and dashed curves designate the distributions in the g, r, and i bands, respectively. The surface brightness was corrected for the foreground reddening in our Galaxy.

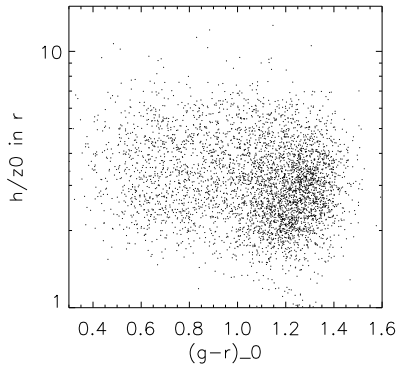

Fig. 7.— The inverse stellar disk thickness h/z_0 (in the r-band) versus the corrected color (g-r) for all galaxies in our sample. The colors are corrected for reddening in our Galaxy.

respectively. It indicates that the galaxies with different asymmetries have mostly the same completeness as the whole our sample of galaxies. We checked if the asymmetry is a function of the disk thickness, central surface brightness, or distance (for those galaxies with available radial velocities), and did not find any such trends. Thus, we select the objects uniformly from the standpoint of their bright - dim halfs asymmetry.

We also sorted out the galaxies by their inverse disk scale ratio h/z_0 in the r band and considered completeness using the V/V_m test. The h/z_0 ranges of (0.0, 2.4), (2.4, 3.1,) (3.1, 3.9), (3.9, 5.1), and over 5.1 made the groups of mostly equal size, and their 95% completeness level starts at the major axis size of 29, 28, 29, 30, and 28 arcsec, respectively. This shows that our sample is not biased over the internal disk thickness.

The galactic colors were estimated using equal areas within the encompassing ellipses. The colors were corrected for the Milky Way reddening using the maps from Schlegel et al. (1998), but they were not corrected for the internal extinction in the galaxies. We do not observe significant trends in the disk thickness with the overall galaxy color, although red objects tend to possess thicker disks, similar to that reported by Kautsch (2009b).

The colors, as well as the bulge-to-disk luminosity ratio, correlate well with the estimated morphological type in our sample, see Fig. 8.

More details on the statistical properties of the derived structural parameters are presented in Table 4.

3.2. The Scale Height Gradient

Since we analyzed the vertical photometric profiles independently of each other, we can estimate how the vertical scale height changes with the distance to the center in terms of the scale height radial gradient. The gradient is calculated from individual vertical photometric profiles in the range from 1 to 3 radial scale lengths. Fig. 9 (lower panel) shows the distribution of the scale height gradient for the whole sample. The gradient was normalized and is shown as $(dz_0/dr)/(h/z_0)$. The distribution peaks close to zero, at small positive values of the gradient: the mean value is 0.063, the median is 0.064, and the mode is 0.067. The fraction of galaxies with strong positive and negative

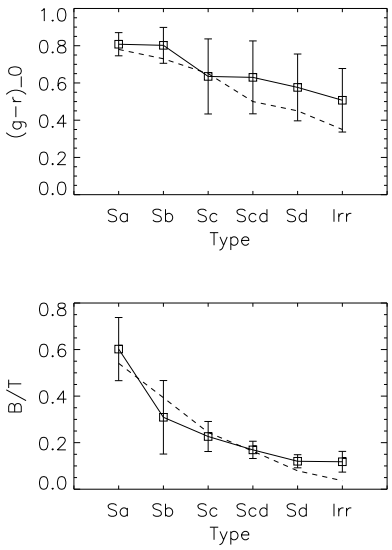

Fig. 8.— The mean values and r.m.s. scatter of the (g-r) color (top) and of the bulge-to-disk luminosity ratio (bottom) for different morphological types in our sample. The dashed curve in the top panel shows the color morphological type dependence for a same of isolated galaxies with arbitrary inclination from (Fernandez Lorenzo et al. 2012). The dashed curve in the bottom panel denotes the bulge-to-total luminosity distribution from EFIGI sample (Baillard et al. 2011).

radial gradients of the z_0 ($\pm$ 0.2 from the median value) is 10.8%. Interesting that large positive gradients of the scale height is observed mostly in the galaxies with significant bulges, whereas bulgeless galaxies have disks without the radial gradients of the vertical scale, on average. This trend suggests that large bulges affect our method of the gradient determination, and the gradients inferred for the galaxies with B/T > 0.4 are biased. For the galaxies with B/T < 0.4 the normalized radial gradient in the r-band is 0.045 on average. Given the bulge contamination and dust effects, we should warn the readers about the limitations of the gradient determination, especially in the case of the smallest galaxies in our sample. The vertical scale gradients can be addressed with additions to a 3-D modeling approach, which we will introduce to the modeling in the next paper.

3.3. The Catalog of True Edge-on Galaxies

We present our sample of edge-on galaxies as an on-line catalog EGIS (Edge-on Galaxies In SDSS) public available at *http://users.apo.nmsu.edu/∼dmbiz/EGIS/* . The catalog's core table is our Table 4, which contains the structural parameters for each image in the g, r, and i bands. The catalog also contains cleaned images used for our analysis of structure, as well as raw (not cleaned) images. All images are trimmed to have the galactic center at the center of the frame and are rotated to place the major axis parallel to the image rows. Note that all initial images for the analysis are taken from the SDSS, so all SDSS data usage policies are applied to our catalog.

Cross-matching over the HyperLeda database allows us to find radial velocities for about 3/4 of our sample. The distribution of the physical properties (the absolute magnitude in the r band, the radial velocity, and the radial and vertical scales in the physical units) is shown in Fig. 10.

The future implications of the catalog include co-adding images in order to study properties the thick disks statistically, evaluation of the bulge properties, and study of scaling relations based on the large sample of similar objects.

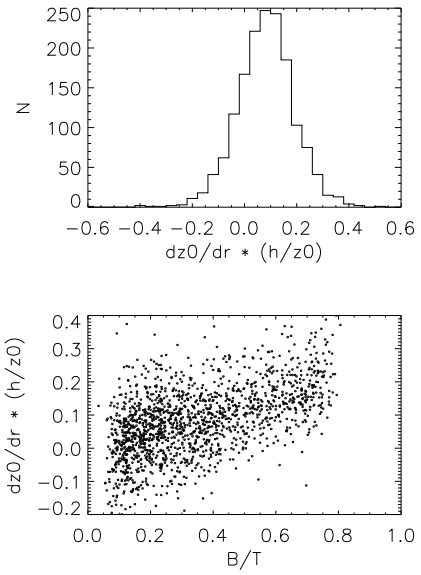

Fig. 9.— Top: The radial gradient of the stellar disk thickness z_0 estimated from the r-band images. The gradient dz_0/dr is normalized by the disk thickness z_0/h. Bottom: the normalized radial gradient of the scale height versus the bulge-to-disk ratio.

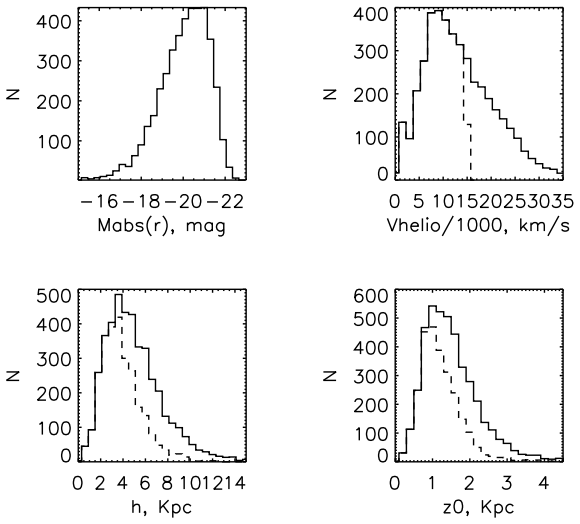

Fig. 10.— The distribution of the absolute magnitude in the r band, radial velocity, and the radial (h) and vertical (z_0) scales expressed in kpc. The absolute magnitude is corrected for reddening in the Milky Way. The h and z_0 distributions for the whole sample are designated by the solid line, whereas the dashed line marks those distributions for relatively nearby galaxies with heliocentric velocity $V_{helio} < 15000$ km/s.

4. Structural Parameters from 3-D Multi-component Modeling

Realistic modeling of edge-on galaxies for the structural parameters determination must include the dust extinction. As modeling of some large galaxies shows (Xilouris et al. 1999; Popescu et al. 2000; Yoachim et al. 2006; Bianchi 2007) the dust in the galaxies can be successfully approximated as embedded disk with uniform extinction and scattering. As Bianchi (2007) noticed, neglecting the dust scattering and taking into account only dust absorption does not introduce significant errors to the resulting structural parameters. We simplify calculations and neglect the dust scattering in the modeling described below and assume that the dust extinction volume density can be expressed as

$$\kappa_{\mathrm{ext},\lambda}(r,z) = \frac{\tau_{0,\lambda}}{2z_{\mathrm{d}}} \exp(-r/h_{\mathrm{d}}) \exp(-|z|/z_{\mathrm{d}}), \tag{2}$$

Here $\tau_{0,\lambda}$ is the face-on optical depth of the dust disk at the center, and h_{d} and z_{d} are the radial and vertical scales of the dust disk. The distribution of the luminosity density in our model stellar disks follows equation (1). We also add a stellar bulge to the modeling since we did not limit our consideration by bulgeless galaxies and many of our galaxies have noticeable bulge (according to Fig. 6 and Table 5). We assume the Hubble volume luminosity density distribution for the bulge (Xilouris et al. 1998), which can be written

$$\rho_{\mathrm{b}}(r,z) = \rho_{0\mathrm{b}}(1-B^2)^{-3/2}\ , \tag{3}$$

where $B = \dfrac{\sqrt{r^2+z^2(b/a)^2}}{R_{\mathrm{e}}}$, $\rho_{0\mathrm{b}}$ is the central luminosity density in the bulge, and R_{e} is the bulge effective radius.

After adding the co-planar embedded extinction disk and tilting the system by close to edge-on inclination angle, we calculate the final brightness distribution via numerical integration of the luminosity volume density along the line-of-sight. The 2-D images were convolved with a Gaussian PSF, same as we used in § 3.

Attempts of modeling the stellar disk using SDSS images with unconstrained set of parameters was performed by Bizyaev (2007) using chi-square minimization of the difference between the real and model galactic images. As modeling of

small samples of well spatially resolved galaxies shows (Xilouris et al. 1999; Matthews et al. 1999; Yoachim et al. 2006; Bianchi 2007), the dust disk described by equation (2) has two times smaller scale height than that in the stellar disks. To simplify calculations, we assume that $z_{\rm d} = z_0/2$ in the further 3-D modeling.

Our model has 14 free parameters: the X-Y position of the center in the sky plane, the position angle of the major axis (PA), the inclination of the galactic plane, central surface brightness and the scales of the stellar disk, central face-on extinction and the scales of the dust disk, and central surface brightness, axes ratio and effective radius of the bulge.

To ensure that we can reliably recover the galactic component parameters, we performed Monte-Carlo simulations and created a set of synthetic images of edge-on galaxies. Using equations (1, 2, 3), we made a large set of synthetic images and projected them to the sky plane by adding some inclination different from the perfect edge-on view and a small position angle tilt. A random noise was added to the images in order to degrade the image quality and to make them have S/N comparable to the observing data. The synthetic images were then evaluated and recovered parameters were compared to the input ones, see Fig. 11.

As the modeling in Fig. 11 shows, not all parameters are recovered equally well: the structural parameters of the stellar disks are the most reliable ones. The dust disk parameters are not reliably estimated. The inclination of the galactic plane is the hardest parameter to estimate even from a smooth and non clumpy synthetic images.

We ran the same simulations with variable pixel size of the synthetic images to understand how small the galaxies could be suitable for the analysis. Fig. 12 demonstrates the stellar disk scales and the central surface brightness (in arbitrary linear units) estimated from synthetic images. We created 21 images for a set of scale heights, and estimated resulting structural parameters from our 1-D and 3-D analysis. As 12 suggests, reliability of both approaches is bad when the scale height is comparable with the pixel resolution in the images. The 1-D analysis overestimates the disk thickness by 15%, given sufficient pixel resolution, which is due to the combination of non-perfect edge-on galactic inclination and effects of the dust

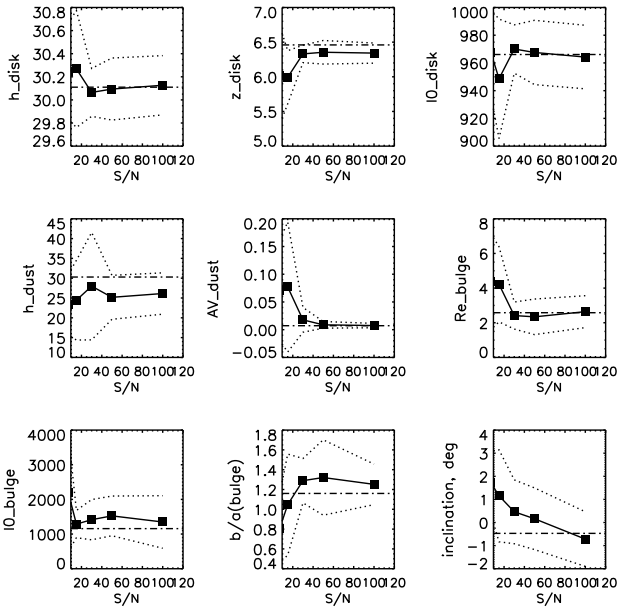

Fig. 11.— The model parameters recovered from our synthetic images. The solid curve with symbols shows the averaged output parameters, The dashed line designates the input value. The dotted lines designate the 1-sigma uncertainty of the parameters estimated from 30 simulations for each S/N ratio.

layer. The difference in the scales determined using these two approaches can be seen in the real data in § 4.1.

The distribution of the radial-to-vertical scale ratio is shown in Fig. 13 for relatively large galaxies (with z_0 >1.2 arcsec). The stellar disks look thinner from the 3-D analysis results in the comparison with Fig. 4. The disk thickness estimated from different bands with the 3-D analysis looks similar. The median inverse disk thickness is 5.7, 5.8, and 5.6 in the g, r, and i bands, respectively.

Since morphological dependence of the stellar disk thickness has been reported from smaller sample studies (de Grijs 1998; Schwarzkopf &Dettmar 2000), we check how the average disk thickness is correlated with our preliminary morphological classification. Figures 14 and 15 compare the median inverse disk thickness estimated for different morphological types. Fig. 14 uses the results of our 1-D analysis, whereas Fig. 15 is based on the results from the 3-D analysis. It can be seen that Fig. 14 is in a very good agreement with figure 6 from de Grijs (1998) (shown with filled circles) and close to the results by Schwarzkopf &Dettmar (2000). Fig. 15 reveals thinner stellar disks in the late-type spiral galaxies. It also suggests that the galactic extinction contributes to the formation of the trend seen in Fig. 14.

The stellar disk structural parameters are estimated for the same galaxies by the 1-D and 3-D approaches independently from each other, so it is worth to compare the resultant parameters. Fig. 16 shows the comparison for the stellar disk scale length h, scale height z_0 and face-on central surface brightness S_0. The vertical scale height in the same images is smaller in the 3-D case, which suggests that taking the dust into consideration improves the analysis. In combination with the correction of the central surface brightness for the internal extinction, our 3-D approach produces significantly brighter stellar disks in the comparison with the 1-D analysis.

Both our 1-D and 3-D approaches to the modeling are affected by limited spatial resolution of SDSS images, which is severe for small galaxies. While deep optical and NIR observations of nearby galaxies allows for seeing very thin and low-contrast disk subsystems as a disk of blue stars reported by Schechtman-Rook & Bershady (2013), most of our galaxies are observed with rather lim-

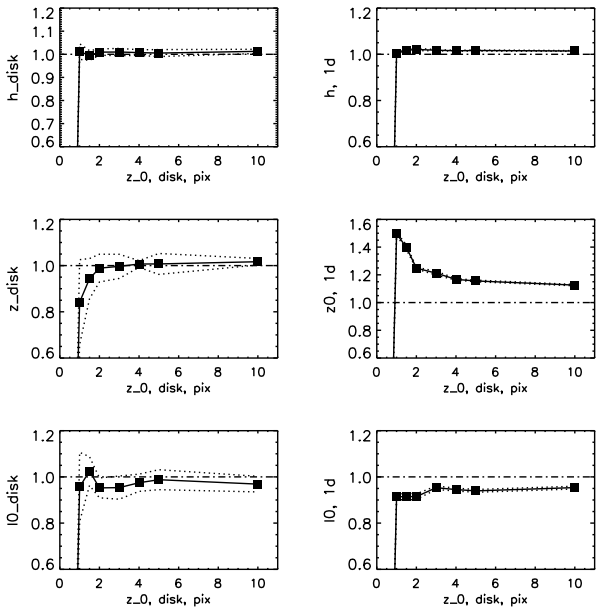

Fig. 12.— The radial and vertical scales and the central surface brightness (in the arbitrary linear units) estimated from synthetic images in dependence of the vertical scale height expressed in pixels. The left-side panels show results of our 3-D analysis, and the right-side panels demonstrate the 1-D analysis. The solid curve with symbols shows the averaged output parameters, The dashed line denotes the input value. The dotted lines designate the 1-sigma uncertainty of the parameters estimated from 21 simulations for each S/N ratio.

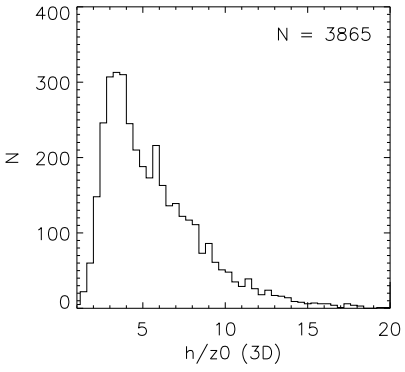

Fig. 13.— The inverse r-band thickness of the stellar disks estimated in our 3-D modeling

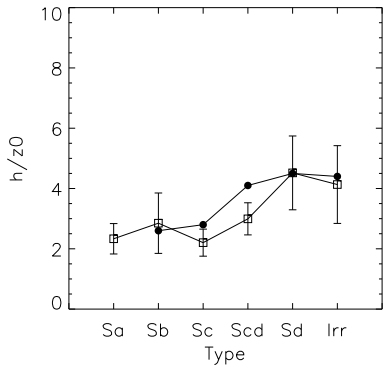

Fig. 14.— The inverse stellar disk thickness for different morphological types in our sample based on our 1-D modeling is shown with the open squares with error bars. The filled circles show the same results by de Grijs (1998).

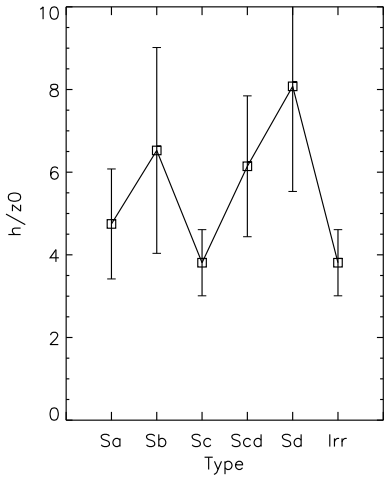

Fig. 15.— The same as Fig. 14 based on our 3-D analysis.

ited resolution (the best SDSS seeing of 1 arcsec corresponds to approximately 1 kpc at 15,000 km/s), which makes study of very thin subsystems impossible with our sample. Same reason prevents us from attempts of selecting the best functional form describing the vertical brightness profiles in thin disks of different galaxies. Fig. 17 demonstrates the relationship between our 1-D and 3-D scale heights. It can be seen that although the trend in Fig. 16 can be described as $z_{0,3D} = 0.58 + 0.94 \cdot z_{0,1D}$, the vertical scales less than ≈ 1 arcsec deviate significantly from this linear relation. Both 1-D and 3-D ways of the scale estimation should be biased for the smallest galaxies in our sample because of the limited angular resolution.

The structural parameters of the stellar disks in the r-band determined with our 3-D modeling approach are shown in Table 6.

Although the amplitude of uncertainties in h/z_0 ratio estimated with our 1-D approach is less than our typical observing errors, we can estimate the systematic addition to the original h/z_0 introduced by the non-perfect edge-on inclination of the galactic midplane to the line of sight. We used the synthetic models developed in §4 and estimated the disk thickness h/z_0 with our 1-D approach with respect to the original one introduced to the artificial models. We ran the synthetic images of edge-on galaxies with added noise (corresponding to SNR = 50 at the center) through our 1-D analysis code. As Fig. 18 shows, deviation of the inclination angle from the perfect 90 degrees introduces a few percent error in the disk thickness estimated with the 1-D approach.

4.1. Limitations to our estimations of the structural parameters

We have to mention the limitations of our analysis of the galactic structure that originates from the limited angular resolution, relatively low signal-to-noise of the data, as well as by simplifications assumed for the analysis.

Possibility of the multi-exponential stellar disk is a next step in complication of our 3-D modeling, together with introducing disk warps and gradi-

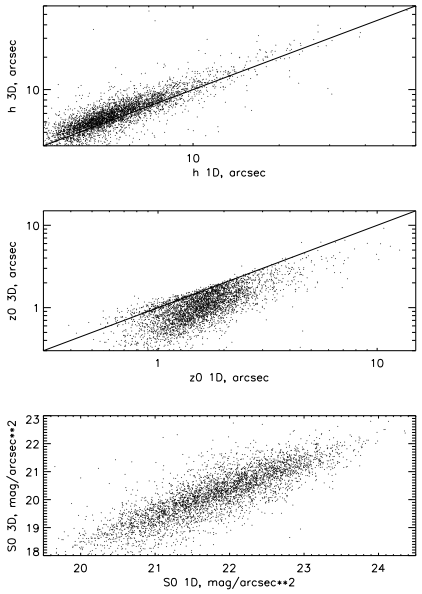

Fig. 16.— Comparison between the structural parameters of the stellar disks estimated via the 3-D modeling and from the 1-D profile analysis. The panels show the radial disk scale length (top), scale height (middle) and the face-on surface brightness (bottom) estimated for the r-band images.

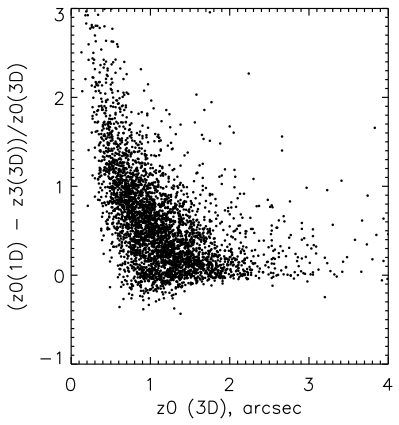

Fig. 17.— The ratio of the stellar disk thickness estimated via the 3-D modeling and from the 1-D profile analysis for the r-band images. While there is a nearly linear dependence for large values, there is a poor agreement between the scales below 1 arcsec.

ents of the disk scale height. Since this cannot be done for the smallest galaxies in the sample, we will consider possibilities for a more complicated modeling in a next paper.

Including the dust scattering into the modeling requires superior quality optical images, and the analysis remains very uncertain unless a multi-wavelength approach is developed (e.g. Baes et al. 2011; Schechtman-Rook et al. 2012). Even in this case the realistic inclusion of the radiative transfer requires careful evaluation of each object individually. Consideration of more sophisticated shortcuts than plain neglecting the dust scattering and clumpy features in the dust layer in the modeling, which can be applied for our large sample, is a goal of our next work in this direction.

A fundamental limitation to our attempt of separating the galactic structural components based on their different spatial scales comes from the fact that the thickness of the stellar disk disk in low-massive galaxies is the same as that of the gas disks. As it was noticed by Dalcanton et al. (2004), disk edge-on galaxies with maximum of the rotation curve less than 120 km/s do not show regular dust lane and look mostly clumpy. Including this fact into our modeling requires kinematic information, or at least availability of the distances for all galaxies in the catalog. We bring consideration of this question out of scope of this paper and notice that our relatively small group morphologically classified as Irr, may mostly consist of such clumpy galaxies.

Our study does not attempt to provide precision modeling for all galactic components, neither select the best individual model description to each object from a variety of available models. Instead it provides a ground for further studies of large samples of edge-on galaxies using both dedicated observations of limited subsamples of certain groups of the galaxies and results from deeper observations that will come from large sky surveys. Incorporating the multi-wavelength information and of kinematic data for a large fraction of the galaxies in our sample will improve the separation of the structural components.

5. Conclusion

Careful selection of candidate galaxies from SDSS images allows us to create the largest mod-

ern sample (5747 objects) of edge-on galaxies ready for further analysis. Our sample is complete for all galaxies with major axis larger than 30 arcsec. The distribution of the the axial ratio shows that our sample size is reasonable, what also confirms its statistical completeness.

We perform a 1-D radial and vertical profile analysis and infer the stellar disk's structural parameters. The results suggest that dust significantly biases the inferred parameters estimated from the optical band images. We also perform a simplified 3-D modeling of all our galaxies taking into account the presence of dust. Comparison between the structural parameters shows that more constrained modeling is needed to eliminate effects of dust in the galaxies.

The catalog can be used for statistical studies of the properties of the thick disks using stacked coadding images. Our large sample makes possible studying scaling relations for galactic stellar disks and bulges.

We thank AAS Small Research grant program and grants RFBR-11-02-12247, RFBR-11-02-00471, RFBR-12-02-00685, and RFBR-14-02-00810 for partial support. Funding for this project was partly provided through the Nova Southeastern University President's Faculty Research and Development Grant. We thank the anonymous referee whose multiple reviews significantly improved the paper.

Funding for SDSS-III has been provided by the Alfred P. Sloan Foundation, the Participating Institutions, the National Science Foundation, and the U.S. Department of Energy Office of Science.

SDSS-III is managed by the Astrophysical Research Consortium for the Participating Institutions of the SDSS-III Collaboration including the University of Arizona, the Brazilian Participation Group, Brookhaven National Laboratory, University of Cambridge, Carnegie Mellon University, University of Florida, the French Participation Group, the German Participation Group, Harvard University, the Instituto de Astrofisica de Canarias, the Michigan State/Notre Dame/JINA Participation Group, Johns Hopkins University, Lawrence Berkeley National Laboratory, Max Planck Institute for Astrophysics, Max Planck Institute for Extraterrestrial Physics, New Mexico State University, New York University, Ohio State University, Pennsylvania State University, University of Portsmouth, Princeton University, the Spanish Participation Group, University of Tokyo, University of Utah, Vanderbilt University, University of Virginia, University of Washington, and Yale University.

We acknowledge the usage of the HyperLeda database (http://leda.univ-lyon1.fr)

REFERENCES

Abadi, M. G., Navarro, J. F., Steinmetz, M., & Eke, V. R., 2003, ApJ, 597, 21

Abazajian, K. N., Adelman-McCarthy, J. K., Ageros, M. A. et al. 2009, ApJS, 182, 543

Aihara, H., Allende Prieto, C., An, D., et al. 2011, ApJS, 193, 29

Baes, M., Verstappen, J., De Looze, I., et al., 2011, ApJS, 196, 22

Bahcall, J.,1984, ApJ, 276, 156

Baillard, A., Bertin, E., de Lapparent, V., Fouqu, P. et al. 2011, A&A, 532, 74

Barbanis, B. & Woltjer, L. 1967, ApJ, 150, 461

Barteldrees, A. & Dettmar, R.-J., 1994, A&AS, 103, 475

Bergvall, N., Zackrisson, E., and Caldwell, B. 2010, MNRAS, 405, 2697

Bianchi, S. 2007, A&A, 471, 765

Bizyaev, D. 2007, BAAS, 39, 758

Bizyaev, D. & Kajsin, S. 2004, ApJ, 613, 886

Bizyaev , D. & Mitronova, S. 2002, A&A, 100, 200

Bizyaev , D. & Mitronova, S. 2009, ApJ, 702, 1567

Bournaud, F., Elmegreen, B. G., & Martig, M. 2009, ApJ, 707, L1

Brook, C. B., Kawata, D., Gibson, B. K., & Freeman, K. C. 2004, ApJ, 612, 894

Brook et al. 2012, MNRAS, 426, 690

Burkert, A., Truran, J. W.' & Hensler, G. 1992, ApJ, 391, 651

Burstein, D. 1979, ApJ, 234, 829

Carlberg, R. G. & Sellwood, J. A. 1985, ApJ, 292, 79

Chen, B., et al. 2001, ApJ, 553, 184

Dalcanton, J. J., & Bernstein, R. A. 2002, ApJS, 124, 1328

Dalcanton, J. J., Yoachim, P., & Bernstein, R. A. 2004, ApJ, 608, 189

De Geyter, G., Baes, M., Fritz, J. & Camps, P. 2013, A&A, 550, 74

de Grijs, R., Peletier, R., & van der Kruit, P. 1997, A&A, 327, 966

de Grijs, R. 1998, MNRAS, 299, 595

de Vaucouleurs, G., de Vaucouleurs, A., Corwin, Jr., H. G., et al. 1991, Third Reference Catalogue of Bright Galaxies (Volume 1-3, Springer-Verlag Berlin Heidelberg New York)

Domenech-Moral, M., Martinez-Serrano, F. J., Dominguez-Tenreiro, R., & Serna, A. 2012 MNRAS, 421, 2510

Fernndez Lorenzo, M., Sulentic, J., Verdes-Montenegro, L., et al. 2012 A&A, 540, 47

Freeman, K. 1970, ApJ, 160, 811

Giovanelli, R., Haynes, M. P., Salzer, J. J., et al. 1994, AJ, 107, 2036

Gunn, J.E., Siegmund, W. A., Mannery, E. J., et al. 2006, AJ, 131, 2332

Hubble, E. 1926, ApJ, 64, 321

Kautsch, S. J. et al, 2006, A&A, 445, 765

Kautsch, S. J., Grebel, E. K., Barazza, F. D., & Gallagher, J. S., III 2006b, A&A, 451, 1171

Kautsch, S. J. 2009, AN, 330, 100

Kautsch, S. J. 2009b, PASP, 121, 1297

Karachentsev, I. D., Karachentseva, V. E., & Parnovskij, S. L., 1993, AN, 314, 97

Karachentsev, I. D., Karachentseva, V. E., Kudrya, Yu. N. et al. 1999, Bull. Spectrosc. Astrophys. Obs., 47, 5

Kormendy, J. & Bruzual, A. G. 1978, ApJ, 223, L63

Kregel, M., van der Kruit, P. , & de Grijs, R. 2002, MNRAS, 334, 646

Kroupa, P. 2002, MNRAS, 330, 707

Kylafis, N. D. & Bahcall J. N. 1987, ApJ, 317, 637

Lintott, C., Schawinski, K., Bamford, S., et al. 2011, MNRAS, 410, 166

Masters, K. L., Nichol, R., Bamford, S. et al. 2010, MNRAS, 404, 792

Matthews, L. D., Gallagher, J. S., & van Driel, W. 1999, AJ, 118, 2751

Mosenkov, A. V., Sotnikova, N. Ya., & Reshetnikov, V.P. 2010, MNRAS, 401, 559

Paturel G., Petit C., Prugniel P., et al. 2003, A&A, 412, 45

Popescu, C. C., Misiriotis, A., Kylafis, N. D., et al. 2000, A&A, 362, 138

Pranger, F., Böhm, A., Ferrari, C., Diaferio, A., Hunstead, R., Maurogordato, S., Benoist, C., Brinchmann, J., & Schindler, S. 2013, A&A, 557, 62

Pohlen, M., Balcells, M, Lutticke, R., & Dettmar, R.-J. 2004, A&A, 422, 465

Qu, Y., Di Matteo, P., Lehnert, M.D., & van Driel, W. 2011, A&A, 530, 10

Samland, M., & Gerhard, O. E. 2003, A&A, 399, 961

Schechtman-Rook, A., Bershady, M. A., & Wood, K. 2012, ApJ, 746, 70

Schechtman-Rook, A. & Bershady, M. A., 2013, arXiv1309.0824

Schlegel, D.J., Finkbeiner, D.P. & Davis, M., 1998, ApJ, 500, 525

Schwarzkopf, U. & Dettmar, R.-J., A&A, 2000, 361, 451

Steinmetz, M. 2003, Ap&SS, 284, 325

Stoughton, C., Lupton, R. H., Bernardi, M. et al. 2002, AJ, 123, 485

Strateva, I., Ivezic, Z., Knapp, G. R. et al. 2001, AJ, 122, 1861

Tissera, P. B., White, S. D. M., & Scannapieco, C. 2012, MNRAS, 420, 255

Thuan, T. X. & Seitzer, P. O. 1979, ApJ, 231, 680

van der Kruit, P. C., Searle, L. 1981, A&A, 95, 105

van der Kruit, P. C., Searle, L. 1981, A&A, 95, 116

Villalobos, A. & Helmi, A. 2008, MNRAS, 391, 1806

Walker, I. R., Mihos, J. C., & Hernquist, L. 1996, ApJ, 460, 121

Xilouris, E. M., Alton, P.B., Davis, J.I. et al 1998, A&A, 331, 894

Xilouris, E. M., Byun, Y. I., Kylafis, N. D., et al. 1999, A&A, 344, 868

Yoachim, P. & Dalcanton, J. J. 2006, AJ, 131, 226

Zasov, A. V., Makarov, D., & Mikhailova, E. 1991, Sov. Astron. Lett., 17, 374

Zibetti, S., White, S. D. M., & Brinkmann, J. 2004, MNRAS, 347, 556

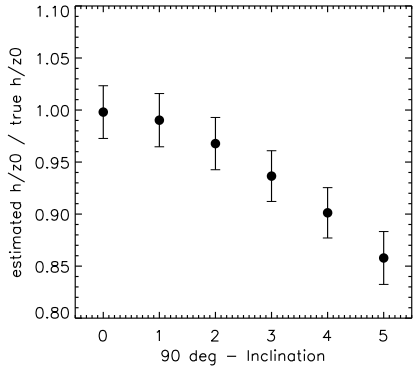

Fig. 18.— The inverse stellar disk thickness h/z_0 estimated with our 1-D approach for a set of synthetic images with introduced non-zero inclination of the galactic midplane. The original model h/z_0 was equal to 4, and there is no dust in the models. The error bars shown in the picture are 10 times expanded and correspond to the models with central SNR = 50.

This 2-column preprint was prepared with the AAS LaTeX macros v5.2.

Table 4

The Structural Parameters of True Edge-on Galaxies From The 1-D Analysis.

Name	band	RA(J2000)	Dec(J2000)	PA	h	dh	z_0	dz_0	S_0	dS_0	grad(z_0)	mag	B/T	Type
EON_0.183_7.090	g	0.182590	7.090147	157.78	7.31	0.61	1.21	0.19	23.75	0.26	-0.194	17.69	0.14	SB
EON_0.183_7.090	i	0.182590	7.090147	157.78	5.56	1.14	1.30	0.20	22.82	0.50	-0.104	16.49	0.18	SB
EON_0.183_7.090	r	0.182590	7.090147	157.78	7.61	2.56	1.31	0.18	23.51	1.04	-0.230	16.88	0.09	SB
EON_0.187_33.757	g	0.186788	33.756809	156.87	2.55	0.17	0.91	0.09	21.80	0.15	0.012	18.23	0.08	SB
EON_0.187_33.757	i	0.186788	33.756809	156.87	3.16	0.06	0.85	0.09	21.30	0.28	-0.048	16.90	0.15	SB
EON_0.187_33.757	r	0.186788	33.756809	156.87	3.59	0.53	0.88	0.10	22.06	0.19	0.061	17.36	0.11	SB
...														

Table is published in its entirety in the electronic edition.

References. — Parameters of the galaxies in the table: EGIS name, SDSS band, RA(J2000) in decimal degrees, Dec(J2000) in decimal degrees, position angle, scale length in arcsec and its uncertainty, scale height in arcsec and its uncertainty, face-on central surface brightness and its uncertainty, vertical gradient of the scale height normalized by the scale ratio ($dz_0/dr * (h/z_0)$), total uncorrected magnitude of the galaxy estimated by integration within the encompassing ellipse, average surface brightness of the galaxy within the encompassed ellipse, the bulge-to-total ratio, mosphological type of galaxies, heliocentric radial velocity in km/s (from LEDA; -1 is inserted if the value is unknown), and an alternative name.

Table 5: The structural parameters derived from the 1-D profile analysis

Parameter	g	r	i
h/z_0	3.57 ± 1.61	3.31 ± 1.31	3.17 ± 1.21
S_0	22.37 ± 0.81	21.56± 0.81	21.10±0.84
B/T	0.24 ± 0.16	0.29 ± 0.17	0.31 ± 0.17
h,arcsec*	5.9 ± 2.3	5.5 ± 2.0	5.3 ± 1.9
z_0,arcsec	1.8 ± 0.6	1.8 ± 0.5	1.8 ± 0.5

Table 5: Mean values and uncertainties of the reverse thickness h/z_0, central surface brightness, and bulge-to-total ratio estimated for different SDSS bands. (*) Median value for the scale length and scale heights in arcsec are given with their uncertainty calculated as 1.48 * MAD (median absolute deviation).

Table 6

The Structural Parameters of True Edge-on Galaxies in the r-band From Our 3-D Analysis.

Name	h	z_0	S_0
EON_113.799_20.000	8.86	1.04	21.34
EON_115.757_45.121	6.53	2.09	19.77
EON_117.764_50.255	3.97	1.13	19.22
EON_119.936_45.366	6.77	1.54	19.46
EON_119.977_47.413	20.66	0.05	20.79
EON_120.940_15.240	4.92	0.03	18.84
...			
Table is published in its entirety in the electronic edition.			

References. — Parameters of the galaxies in the table: EGIS name (same as in Table 4), scale length in arcsec, scale height in arcsec, and face-on central surface brightness in the r-band (mag arcsec^{-2}).